Computerized segmentation of whole-body bone scintigrams and its use in automated diagnostics

Luka Šajn[1], Matjaž Kukar[1], Igor Kononenko[1], Metka Milčinski[2]

[1]University of Ljubljana
Faculty of Computer and Information Science
Tržaška 25, SI-1001 Ljubljana, Slovenia
{luka.sajn, igor.kononenko}@fri.uni-lj.si

[2]University Medical Centre in Ljubljana
Department for Nuclear Medicine
Zaloška 7, SI-1525 Ljubljana, Slovenia
metka.milcinski@kclj.si

20th May 2005

Author responsible for correspondence: Luka Šajn[1], tel. +386 41 795 980

Abstract

Bone scintigraphy or whole-body bone scan is one of the most common diagnostic procedures in nuclear medicine used in the last 25 years. Pathological conditions, technically poor image resolution and artifacts necessitate that algorithms use sufficient background knowledge of anatomy and spatial relations of bones in order to work satisfactorily. A robust knowledge based methodology for detecting reference points of the main skeletal regions that is simultaneously applied on anterior and posterior whole-body bone scintigrams is presented. Expert knowledge is represented as a set of parameterized rules which are used to support standard image processing algorithms. Our study includes 467 consecutive, non-selected scintigrams, which is, to our knowledge the largest number of images ever used in such studies. Automatic analysis of whole-body bone scans using our segmentation algorithm gives more accurate and reliable results than previous studies. Obtained reference points are used for automatic segmentation of the skeleton, which is applied to automatic (machine learning) or manual (expert physicians) diagnostics. Preliminary experiments show that an expert system based on machine learning closely mimics the results of expert physicians.

Keywords: whole-body bone scintigraphy, reference point detection, automatic segmentation, image processing, machine learning

1 Introduction

Whole-body scan or bone scintigraphy is a well known clinical routine investigation and one of the most frequent diagnostic procedures in nuclear medicine[1]. Indications for bone scintigraphy include benign and malignant diseases, infections, degenerative changes [2]. Bone scintigraphy has high sensitivity and the changes of the bone metabolism are seen earlier than changes in bone structure detected on radiographs [1].

The investigator's role is to evaluate the image, which is of poor resolution due to the physical limitations of gamma camera. There are approximately 158 bones visible on both anterior and posterior whole-body scans [3]. Poor image resolution and the number of bones to inspect make the evaluation of images difficult. Some research on automating the process of counting the bone lesions has been done, but only a few studies attempted to automatically segment individual bones prior to the computerized evaluation of bone scans [4; 5; 6].

1.1 Related work

First attempts to automate scintigraphy in diagnostics for thyroid structure and function were made in 1973 [7]. Most of the research on automatic localization of bones has been done at the former Institute of medical information science at the University of Hildesheim in Germany from 1994 to 1996. The main contribution was made by Berning [5] and Bernauer [4] who developed semantic representation of the skeleton and evaluation of the images. Benneke [6] has realized their ideas in 1996.

Yin and Chiu [8] tried to find lesions using a fuzzy system. Their preprocessing of scintigrams includes rough segmentation of six parts with fixed ratios of the whole skeleton. Those parts are rigid and not specific enough to localize a specific bone. Their approach for locating abnormalities in bone scintigraphy is limited to point-like lesions with high uptake.

When dealing with lesion detection other authors like Noguchi [3] have been using intensity thresholding and manual lesion counting or manual bone ROI (region of interest) labelling. Those procedures are only sufficient for more obvious pathologies whereas new emerging pathological regions are overlooked.

2 Aim and our approach

In everyday practice, when a bone is observed, it is diagnosed by the expert physician according to several possible pathologies (lesions, malignom, metastasis, degenerative changes, inflammation, other pathologies, no pathologies). Some pathologies are obvious and could be found even by a less experienced observer, but most are not and sometimes missed even by a specialists. Therefore this process can be supported by using some machine learning classifier [9] which produces independent diagnoses. As an input a suitably parameterized bone image is given, obtained from detected reference points. Output assigns

the bone to one of the above pathologies. It can be therefore used as a tool to give physician an additional insight in the problem.

The aim of our study was to develop a robust method for segmenting whole-body bone scans to allow further development of automatic algorithms for bone scan diagnostics of individual bones.

In order to achieve a robust reference point detection, we have developed the algorithm for detecting extreme edges in the image (peaks). The experience with automatic processing is presented. Several image processing algorithms are used such as binarization, skeletonization, Hough's transform, Gaussian filtering [10], least square method and ellipse fitting in combination with background knowledge of anatomy and scintigraphy specialities.

3 Materials and methods

3.1 Patients and images

Retrospective review of 467 consecutive, non-selected scintigraphic images from 461 different patients who visited University Medical Centre in Ljubljana from October 2003 to June 2004 was performed. Images were not preselected, so the study included standard distribution of patients coming to examination in 9 months. 19% of the images were diagnosed as normal, which means no pathology was detected on the image. 57% of the images were diagnosed with slight pathology, 20% with strong pathology and 2% were classified as super-scans.

Images also contained some artifacts and non-osseous uptake such as urine contamination and medical accessories (i.e. urinary catheters) [11]. In addition, segmentation was complicated by the radiopharmaceutical site of injection. Partial scans (missing a part of the head or upper/lower extremities in the picture) were the case in 18% of the images. There were also adolescents with growth zones (5% of the images), manifested as increased osteoblastic activity in well delineated areas with very high tracer uptake.

3.2 Bone scintigraphy

All patients were scanned with gamma camera model Siemens MultiSPECT with two heads with LEHR (Low Energy High resolution) collimators. Scan speed was 8cm per minute with no pixel zooming. 99m-Tc-DPD (Techneos^R) was used. Bone scintigraphy was obtained about 3h after intravenous injection of 750 MBq of radiopharmaceutical agent. The whole body field was used to record anterior and posterior views digitally with resolution of 1024 x 256 pixels. Images represent the counts of detected gamma rays in each spatial unit with 16-bit grayscale depth.

3.3 The Algorithm

In order to make the detection of reference points faster and more reliable we have tried to automatically detect intuitive peaks which would represent edges and would cover roughly also the reference points. With normal Canny edge filter too many peaks were obtained. Our approach is based on orthogonal two-way Gaussian filtering [12]. The algorithm (1) works as shown in the pseudo-code.

3.4 Detection of reference points

Bone scans are very different (Figure 1) one from another even though the structure and position of bones is more or less the same. In practice many scans are only partial because only a determined part of the body is observed or due to the scanning time limitations. In our study we have observed that only on two images out of 467 the shoulders were not visible. Many other characteristic parts could have been missing in images more often (i.e. head, arms, one or both legs). Therefore as the main reference points to start with, which means they are supposed to be visible in the images, shoulders have been chosen. Second and the last assumption is the upward orientation of the image. This assumption is not limiting since all scintigraphies are made with the same orientation.

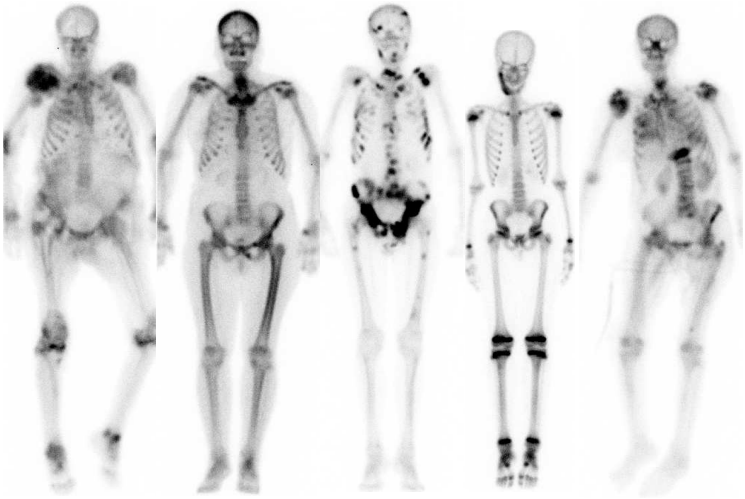

Figure 1: Examples of body scan variety

Low image intensities (count level) acquired in typical studies are due to the limited level of radioactive dosage required to ensure patient's safety. This causes distorted image of bone scans. Bone edges are more expressive after images are filtered with some averaging algorithm (i.e. wavelet based, median

Algorithm 1 Detect relevant peaks Ω

Require: original image $I[x_i, y_j], i \in [0, m-1], j \in [0, n-1]$; Gaussian filter $G_{3\times 3}\left(\frac{1}{16}\begin{bmatrix} 1 & 2 & 1 \\ 2 & 4 & 2 \\ 1 & 2 & 1 \end{bmatrix}\right)$; averaging window $W_{w\times h}$; minimal peak distance d

Ensure: relevant set of peaks Ω

$I_1 \Leftarrow I \times G$ {Gaussian filter applied}
$i \leftarrow 0, j \leftarrow 0, I_2 \Leftarrow 0$
for $i < m$ **do**
  for $j < n$ **do**
    for each point $p_{a,b}$ in W around the center $I_{1(i,j)}$ **do**
      $I_{2(i,j)} \Leftarrow I_{2(i,j)} + (I_{2(a,b)} * (\frac{w+h}{2} - 1 - (|i-a| + |j-b|)))$
    end for
  end for
end for
{normalize intensities}
$\forall (i,j) \in [0..m-1] \times [0..n-1] : I_{2(i,j)} \leftarrow I_{2(i,j)}/(\frac{w+h}{2} - 1)$
$i \leftarrow 1, j \leftarrow 0, \Omega_1 \Leftarrow \{\}$
{vertical pass to calculate horizontal peaks}
for $i < n-1$ **do**
  for $j < m$ **do**
    if $I_{2(i-1,j)} < I_{2(i,j)} > I_{2(i+1,j)}$ **then**
      $\Omega_1 = \Omega_1 \cup \{I_{2(i,j)}\}$
    end if
  end for
end for
$i \leftarrow 0, j \leftarrow 1$
{horizontal pass to calculate vertical peaks}
for $j < m-1$ **do**
  for $i < n$ **do**
    if $I_{2(i,j-1)} < I_{2(i,j)} > I_{2(i,j+1)}$ **then**
      $\Omega_1 = \Omega_1 \cup \{I_{2(i,j)}\}$
    end if
  end for
end for
$\Omega \Leftarrow \{\}$
sort Ω_1 by element intensities
for $\forall$ element el in Ω_1 **do**
  if minimal distance of el to $\Omega > d \vee \Omega = \{\}$ **then**
    $\Omega = \Omega \cup el$
  end if
end for

filter, Gaussian filter) [10]. A Gaussian filter is used so that the detection of peaks is more reliable (comparisons in lines 16 and 25 detect peaks better). The size of the averaging window $W_{w\times h}$ was experimentally set to 11×5 for it gave best results by the means of segmentation accuracy. In the case of scintigraphic images there is no problem with introducing scale variant methods since the nature of this image modality guaranties a fixed scale (100 pixels $\approx 24cm$).

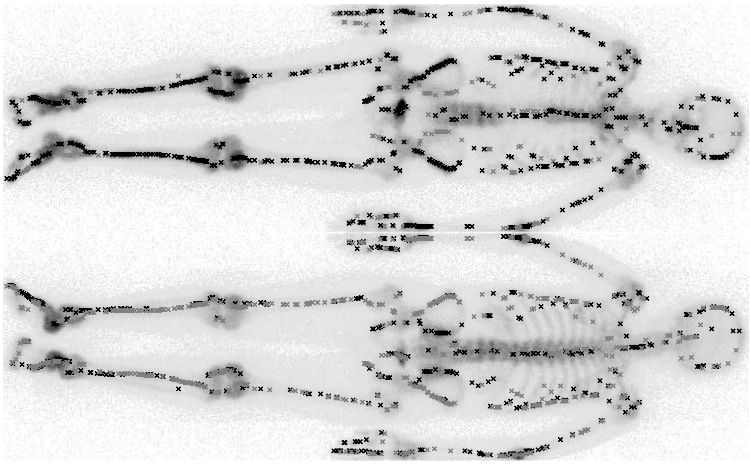

Figure 2: Example of detected image peaks on anterior and posterior image using the algorithm 1

With the use of the detected peaks (Figure 2) the reference points are searched for. Both images, anterior and posterior, are simultaneously processed in the same detection order and in each step the detected reference points visible on both images are compared. Detected points from the anterior image are mirrored to the posterior and vice versa. Some bones are better visible on anterior and some on posterior images due to the varying distances from both collimators. Mirrored points improve the calculation of circles, lines and ellipses with least square method (LSM) since the main bones have the same shape and position on both images.

The order in which the reference points were detected was determined using knowledge of human anatomy as well as physicians' recommendations. They are represented as a list of parameterized rules. Rule parameters (e.g. thresholds, spatial and intensity ratios) were initially set by physicians and further refined on a separate tuning set. More details can be found in [12].

Respective skeletal regions are processed in the following order: shoulders, pelvis, head, thorax and extremities.

3.4.1 Shoulders.

The algorithm searches for the highest detected peak on both sides of the image. The next step is to locally shift the candidate points with local maximum in-

tensity tracing to the outermost location. Only in 5 images out of 467 shoulders were not found correctly due to the tilted head position.

3.4.2 Pelvic region (ilium bone, pubis bone, great trochanter of femur).

The most identifiable bone in pelvic region is the ilium bone which has higher uptake values than it's neighboring soft tissue. The ilium bone has a circular shape in the upper part and it is therefore convenient for circle detection with LSM. This bone is well described with already detected peaks as shown in Figure 3(b). The ilium position is roughly estimated with regions of interest (ROIs) which are found on the basis of the skeleton's anticipated ratios and reference points found up to this step of detection.

The pelvis is located at the end of the spine and has approximately the same width as shoulders. In order to find the pelvis, the calculation of the spine position is required. This is done with a beam search (Figure 3(a)). The anticipated spine length is determined from the distance between shoulders. Beam starting point is the middle point of the shoulders and it's orientation is perpendicular to the shoulder line. The angle at which the beam covers most peaks is a rough estimation of spine direction since there is most of the uptake in the vertebrae and hence peaks are dense in that region.

The pubis bone is detected by estimating the pubis ROI using detected ilium location, distance between detected ilium circles and their inclination. The experimentally determined ROI's size is narrowed and additional vertical peaks are added and circles detected as shown in Figure 3(b).

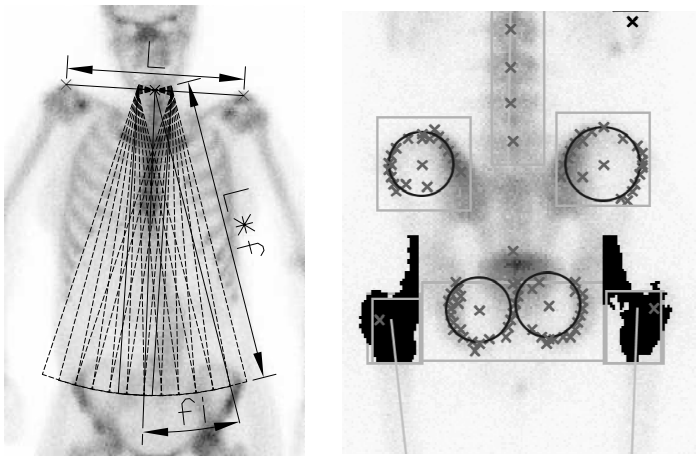

(a) Beam search sketch (b) Detection of bones in the pelvic region

Figure 3: Beam search and detection in pelvic region

3.4.3 Head and neck.

When at least the image orientation and the location of the shoulders are known, some part of the neck or even head is visible since they are between the shoulders. Finding the head is not difficult but its orientation is, especially in cases where a part of the head in scan is not visible. The most reliable method for determining head orientation and position is ellipse fitting of the head contour determined by thresholding.

The general quadratic equation for an ellipse in xy-plane is a second order polynomial

$$a_{11}x^2 + 2a_{12}xy + a_{22}y^2 + b_1x + b_2y + c = 0 \tag{1}$$

All conic sections are represented by this equation. The ellipses are those for which $a_{11}a_{22} - a_{12}^2 > 0$. It can be shown [13] that using this restriction the center of an ellipse $C(k_1, k_2)$ is given by the following equation

$$C(k_1, k_2) = \frac{(a_{22}b_1 - a_{12}b_2, a_{11}b_2 - a_{12}b_1)}{2(a_{12}^2 - a_{11}a_{22})}. \tag{2}$$

The main axes and orientation can be expressed with polynomial coefficients.

Let $\mu = 1/(a_{11}k_1^2 + 2a_{12}k_1k_2 + a_{22}k_2^2 - c)$ and define $m_{11} = \mu a_{11}, m_{12} = \mu a_{12}$, and $m_{22} = \mu a_{22}$. Set $\lambda_1 = ((m_{11} + m_{22}) + \sqrt{(m_{11} - m_{22})^2 + 4m_{12}^2})/2$. The semiminor axis b of the ellipse is $b = \frac{1}{\sqrt{\lambda_1}}$. The semimajor axis is calculated in similar way. Set $\lambda_2 = ((m_{11} + m_{22}) - \sqrt{(m_{11} - m_{22})^2 + 4m_{12}^2})/2$. The semimajor axis a is $a = \frac{1}{\sqrt{\lambda_2}}$.

The angle formed by the major axis with the positive x-axis Θ satisfies the equation $\tan(2\Theta) = -\frac{a_{12}}{a_{22} - a_{11}}$.

Equation 1 can be solved using the least square method and from obtained coefficients all ellipse parameters representing head can be expressed. The experiments showed (Figure 4) very good results regarding head orientation and hence detection of the neck.

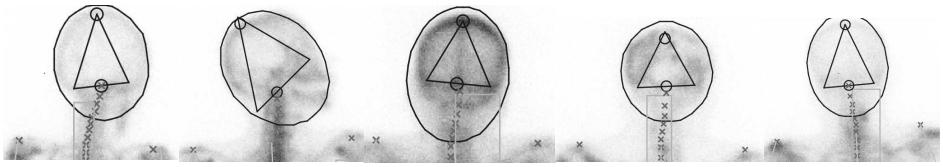

Figure 4: Examples of head detections in various orientations

Neck is found by local vertical shifting of a stripe determined by the ellipse's semiminor axis (position and orientation).

3.4.4 Thoracic part (vertebrae, ribs).

Vertebrae have more or less constant spatial relations, the only problem is that on a bone scintigraphy only a planar projection of the spine is visible. Since the spine is longitudinally curved, the spatial relations vary due to different longitudinal orientation of the patients. Average vertebrae relations have been experimentally determined from normal skeletons.

Ribs are the most difficult skeleton region to detect since they are quite unexpressive on bone scans, their formation can vary considerably and their contours can be disconnected in the case of stronger pathology (Figure 5).

Many contour following techniques (i.e. 'turtle' procedure, crack following, border following ... [14]) exist in image processing but they all require a connected shape of the searched object. For rib contour detection we use morphology based image operations instead, particularly three well known algorithms (dynamic binarization, skeletonization [15] and Hough transform [16]).

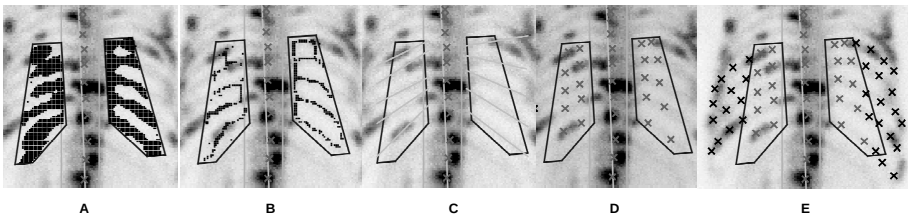

Figure 5: Rib detection steps example on a skeleton with strong pathology. Rib ROI is binarized (A), binarized image is skeletonized (B), Hough transform of linear equation is calculated on skeleton points (C), reference points are estimated using results of the Hough transform (D), rib contours are individually followed by the contour following algorithm which uses background knowledge of anticipated rib shape (E).

3.4.5 Lower and upper extremities (femur, knee, tibia, fibula, humerus, elbow, radius, ulna).

These extremities are often partly absent from whole-body scan because of limited gamma camera detector width. In our patients, a maximum of 61cm width is usually not enough for the entire skeleton. The regions of humerus, ulna and radius as well as femur, tibia and fibula bone are located with the use of controlled beam search. The beam lengths can be estimated from skeletal relationships (i.e. femur length is estimated as 78% of the distance between the neck and ilium bone center). The detection is designed so that a part or all of the extremities and/or the head may not be visible.

3.5 Diagnosing pathologies with machine learning

When all reference points are obtained, every bone is assigned a portion of original scintigraphic image, according to relevant reference points. Obtained images were parameterized using the ArTeX algorithm [17]. It uses association rules to describe images in a rotation-invariant manner. Rotation invariance is very important in this case since it accounts for different patients' positions inside the camera.

Bones were described with several hundreds of automatically generated attributes. They were used for training the SVM [18] learning algorithm. In our preliminary experiments pathologies were not discriminated, i.e. bones were labelled with only two possible diagnoses (no pathology, pathology). In 19% of patients no pathology or other artifacts were detected by expert physicians. In the remaining 81% of the patients at least one pathology or artifact was observed.

4 Results

4.1 Segmentation

Approximately half of the available images were used for tuning rule parameters to optimize the recognition of the reference points and another half to test it. All 246 patients examined from October 2003 to March 2004 were used as the tuning set and 221 patients examined from April 2004 to June 2004 were used as the test set. In the tuning set there were various non-osseous uptakes in 38.9% of the images, 47.5% images with the visible injection point and 6.8% images of adolescents with the visible growth zones. Similar distribution was found in the test set (34.5% non-osseous uptakes, 41.0% visible injection points and 2.85% adolescents). Most of the artifacts were minor radioactivity points from urine contamination in genital region or other parts (81.4% of all artifacts) whereas only few other types were observed (urinary catheters 13%, artificial hips 4% and lead accessories 1.6%). We have observed that there were no ill-detected reference points in adolescents with the visible growth zones since all the bones are homogenous, have good visibility and are clearly divided with growth zones. Results of detecting reference points on the test set are shown in the Table 1.

The algorithm was implemented in a system called "Skeleton 1.0" (written in Java 2 (SE) v 1.4.2) (Figure 6). The current system includes image editing, filtering with different linear filters, conversions to other formats, region localization using the scalable correlation, storing images in database with batch procedures, XML exports of reference points, manual correction of reference points and image annotation. All high complexity algorithms were avoided and used algorithms were optimized in the sense of computational complexity. So the detection of reference points on both anterior and posterior image takes approximately 3s on Pentium 4, 2.8GHz, 1GB RAM.

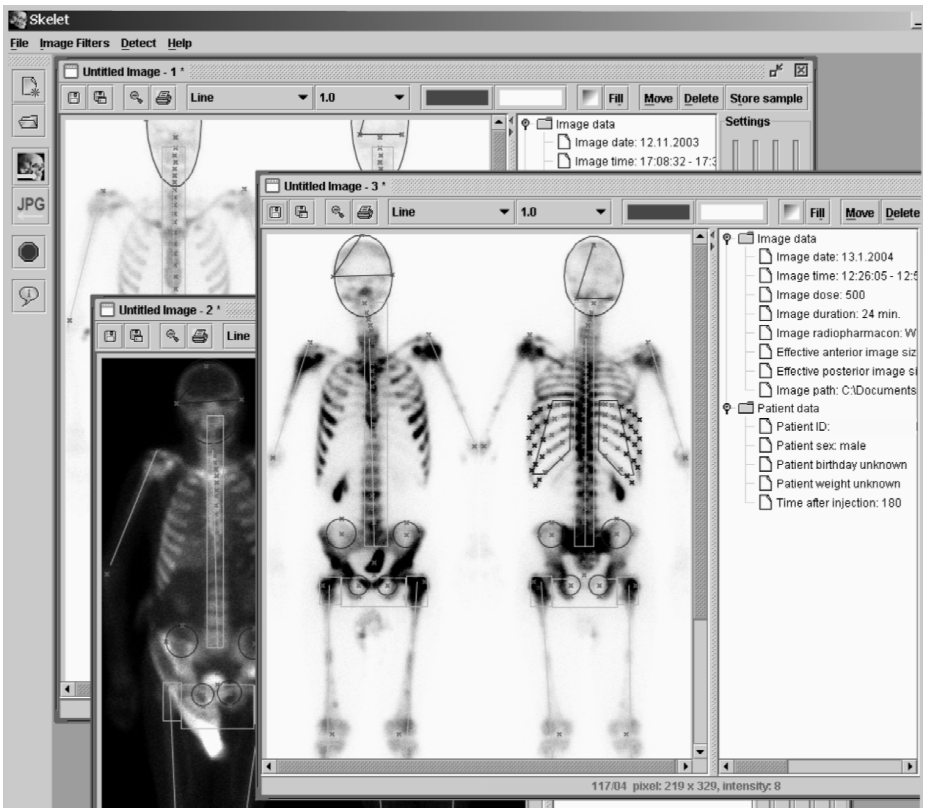

Figure 6: View of the program "Skeleton"

4.2 Machine learning results

From our complete set of 467 patients, pathologies were thoroughly evaluated by physicians only for 268 patients. These 268 patients were used for evaluation of machine learning approach by using ten-fold cross validation. Results are shown in Table 2. They are quite impressive, given high numbers of different bones (158 visible for an individual adult patient). The bones were grouped in ten relevant groups whereas for preliminary classification those groups were divided only in pathological and normal classes.

5 Discussion

The testing showed encouraging results since the detection of proposed reference points gave excellent results for all bone regions but the extremities, which was expected.

Special attention has been paid to the images with partial skeletons since this is often the case in clinical routine (in our study 18% of the images were partial and no particular problem appeared in detecting) and a robust segmentation algorithm should not fail on such images. As expected, the detection of ribs showed to be the most difficult. The results show that in 14% to 20% of images there were difficulties in detecting the ribs. This usually means one rib is missed or not followed to the very end which we intend to improve in the future. In the present system (Figure 6) such reference points can be manually repositioned by the expert physicians.

The automatically detected reference points can be used for mapping a standard skeletal reference mask, which to our belief, is the best way to find individual bones on scintigrams since bone regions are often not expressive enough to follow their contour. An example of such mask mapping and extracted bones is shown in Figure 7(a) and 7(b).

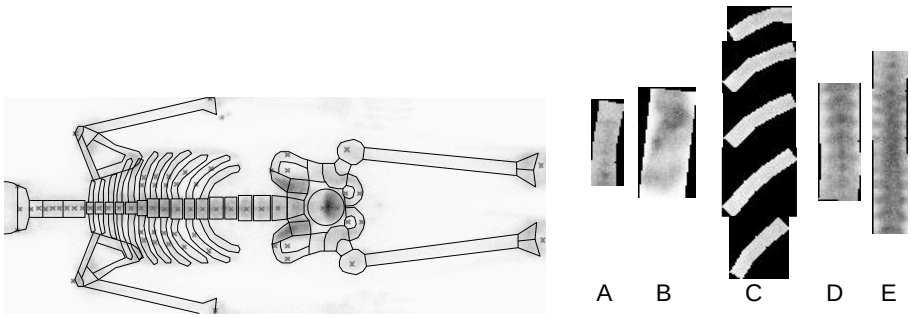

(a) Example of mapped standard skeletal mask with the detected reference points

(b) Examples of clipped bones (A - cervical spine, B foot, C - ribs, D - lumbal spine, E - thoracic spine)

Figure 7: Using reference points for bone extraction

While our experimental results with machine learning are quite satisfactory, one must bear in mind that they were obtained for a simplified (two class) problem. In our case simply extending a problem to a multi-class paradigm is not acceptable, since the bone may be assigned several different pathologies at the same time. In our new approach which we are currently developing, the problem will be rephrased to the multi-label learning problem where each bone will be labelled with a nonempty subset of all possible labels [19; 20].

6 Conclusion

The presented computer-aided system for bone scintigraphy is a step forward in automating routine medical procedures. Some standard image processing algorithms were tailored and used in combination to achieve the best reference

point detection accuracy on scintigraphic images which have very low resolution. Because of poorer image resolution compared to conventional radiography, the presence of artifacts and pathologies necessitate that algorithms use as much background knowledge on anatomy and spatial relations of bones as possible in order to work satisfactorily. This combination gives quite good results and we expect that further studies on automatic scintigraphy diagnosing using reference points for image segmentation will give more accurate and reliable results than previous studies, negligent to the segmentation.

This approach opens a new view on automatic scintigraphy evaluation, since in addition to detection of point-like high-uptake lesions there are also:

- more accurate and reliable evaluation of bone symmetry when looking for skeletal abnormalities. Many abnormalities can be spotted only when the symmetry is observed (differences in length, girth, curvature etc.),
- detection of lesions with low-uptake or lower activity due to metallic implants,
- possibility of comparing uptake ratios among different bones,
- more complex pathology detection with combining pathologies of more bones (i.e. arthritis in joints)
- possibility of automatic reporting of bone pathologies in written language.

Although the machine learning approach described in this work is in an early stage of development it is already in routine use at the University Medical Centre in Ljubljana, Slovenia. However, preliminary results are encouraging and switching to the multilabel learning framework may make them even better.

Acknowledgement

This work was supported by the Slovenian Ministry of Higher Education, Science and Technology through the research programme P2-0209. Special thanks to nuclear medicine specialist Jure Fettich at the University Medical Centre in Ljubljana for his help and support.

Table 1: **Number of incorrectly detected reference points on the test set. Both frequencies and percentages are given.**

Bone	*no pathology*		*slight pathology*		*strong pathology*		*super-scan*		all	
females	*22*		*78*		*15*		*1*		*116*	
ilium	0		2	1.7%	2	1.7%	1	0.9%	5	4.3%
pubis	0		2	1.7%	1	0.9%	0		3	2.6%
trochanter	0		1	0.9%	0		0		1	0.9%
shoulder	0		0		1	0.9%	0		1	0.9%
extremities	1	0.9%	4	3.4%	0		0		5	4.3%
spine	0		0		1	0.9%	0		1	0.9%
ribs	6	5.2%	8	6.9%	3	2.6%	0		17	14.7%
neck	0		2	1.7%	0		0		2	1.7%
males	*24*		*55*		*24*		*2*		*105*	
ilium	0		0		4	3.8%	0		4	3.8%
pubis	2	1.9%	1	1.0%	1	1.0%	0		4	3.8%
trochanter	0		0		0		0		0	
shoulder	0		0		0		0		0	
extremities	4	3.8%	7	6.7%	0		0		11	10.5%
spine	0		2	1.9%	0		0		2	1.9%
ribs	5	4.8%	9	8.6%	0		0		14	13.3%
neck	2	1.9%	2	1.9%	0		0		4	3.8%
sum	*46*		*133*		*39*		*3*		*221*	
ilium	0		2	0.9%	6	2.7%	1	0.5%	9	4.1%
pubis	2	0.9%	3	1.4%	2	0.9%	0		7	3.2%
trochanter	0		1	0.5%	0		0		1	0.5%
shoulder	0		0		1	0.5%	0		1	0.5%
extremities	5	2.3%	11	5.0%	0		0		16	7.2%
spine	0		2	0.9%	1	0.5%	0		3	1.4%
ribs	11	5.0%	17	7.7%	3	1.4%	0		31	14.0%
neck	2	0.9%	4	1.8%	0		0		6	2.7%

Table 2: Experimental results with machine learning on two-class problem.

Bone group	Classification accuracy %	spec.%	sensit.%
Cervical spine	75,9	80,0	77,8
Feet	83,8	84,1	68,0
Skull posterior	94,7	88,2	100,0
Ilium bone	87,3	87,6	82,8
Lumbal spine	71,4	75,7	65,4
Femur and tibia	88,9	84,6	73,3
Pelvic region	92,2	90,7	85,0
Ribs	98,1	92,5	91,7
Scapula	91,4	90,9	90,9
Thoracic spine	82,0	79,2	61,5
Average	**86,6**	**85,4**	**79,6**

References

[1] Müller V., Steinhagen J., de Wit M., and Bohuslavizki H. K. Bone Scintigraphy in Clinical Routine. *Radiol Oncol*, 35(1):21–30, 2001.

[2] Hendler A. and Hershkop M. When to Use Bone Scintigraphy. It Can Reveal Things Other Studies Cannot. *Postgraduate Medicine*, 104(5):54–66, 11 1998.

[3] Noguchi M., Kikuchi H., Ishibashi M., and Noda S. Percentage of the Positive Area of Bone Metastasis is an Independent Predictor of Disease Death in Advanced Prostate Cancer. *British Journal of Cancer*, (88):195–201, 2003.

[4] Bernauer J. Zur Semantischen Rekonstruktion Medizinischer Begriffssysteme. Habilitationsschrift, Institut für Medizinische Informatik, Univ. Hildesheim, 1995.

[5] Berning K.-C. *Zur Automatischen Befundung und Interpretation von Ganzkörper-Skelettszintigrammen.* PhD thesis, Institut für Medizinische Informatik, Universität Hildesheim, 1996.

[6] Benneke A. Konzeption und Realisierung Eines Semi-Automatischen Befundungssystems in Java und Anbindung an ein Formalisiertes Begriffssystem am Beispiel der Skelett-Szintigraphie. Diplom arbeit, Institut für Medizinische Informatik, Universität Hildesheim, mentor Prof. Dr. D.P. Pretschner, 1997.

[7] Maisey M.N., Natarajan T.K., Hurley P.J., and Wagner H.N. Jr. Validation of a Rapid Computerized Method of Measuring 99mTc Pertechnetate Uptake for Routine Assessment of Thyroid Structure and Function. *J Clin Endocrinol Metab*, 36:317–322, 1973.

[8] Yin T.K. and Chiu N.T. A Computer-Aided Diagnosis for Locating Abnormalities in Bone Scintigraphy by a Fuzzy System With a Three-Step Minimization Approach. *IEEE Transactions on Medical Imaging*, 23(5):639–654, 5 2004.

[9] Kukar M., Kononenko I., Grošelj C., Kralj K., and Fettich J. Analysing and Improving the Diagnosis of Ischaemic Heart Disease with Machine Learning. *Artificial Intelligence in Medicine*, 16:25–50, 1999.

[10] Jammal G. and Bijaoui A. DeQuant: a Flexible Multiresolution Restoration Framework. *Signal Processing*, 84(7):1049–1069, 7 2004.

[11] Weiner M. G., Jenicke L., Mller V., and Bohuslavizki H. K. Artifacts and Non-Osseous Uptake in Bone Scintigraphy. Imaging Reports of 20 Cases. *Radiol Oncol*, 35(3):185–91, 2001.

[12] Šajn L., Kononenko I., Fettich J., and Milčinski M. Automatic Segmentation of Whole-Body Bone Scintigrams. Technical report, Faculty of Computer and Information Science, University of Ljubljana, Nov. 2004.

[13] Eberly D. Information about ellipses. Magic Software, Inc., 12 2003.

[14] Kindratenko V. *Development and Application of Image Analysis Techniques for Identification and Classification of Microscopic Particles*. PhD thesis, Universitaire Instelling Antwerpen, Departement Scheikunde, 1997.

[15] Blum H. *Models for the Perception of Speech and Visual Form*. MIT Press, 1967.

[16] Hough P.V.C. Machine analysis of bubble chamber pictures. International Conference on High Energy Accelerators and Instrumentation, CERN, 1959.

[17] Bevk M. and Kononenko I. Towards Symbolic Mining of Images with Association Rules: Preliminary Results on Textures. In Brito P. and Noirhomme-Fraiture M., editors, *ECML/PKDD 2004: proc. of the workshop W2 on symbolic and spatial data analysis: mining complex data structures*, pages 43–53, 2004.

[18] Cristianini N. and Shawe-Taylor J. *An Introduction to Support Vector Machines and Other Kernel-Based Learning Methods*. Cambridge University Press, 2000.

[19] Shen X., Boutell M., Luo J., and Brown C. Multi-Label Machine Learning and its Application to Semantic Scene Classification. In *Proceedings of the 2004 International Symposium on Electronic Imaging (EI 2004)*, San Jose, California, 2004.

[20] McCallum A. Multi-Label Text Classification with a Mixture Model Trained by EM. In *Proc. AAAI'99 Workshop on Text Learning*, 1999.